Temperature dependent infrared absorption, crystal-field and intensity analysis of Ce^{3+} doped $LiYF_4$

Jon-Paul R. Wells[a,b,*], Sebastian P. Horvath[a], Michael F. Reid[a,c]

[a] *The Dodd-Walls Centre for Quantum and Photonic Technologies and Department of Physics and Astronomy, University of Canterbury, PB4800, Christchurch 8140, New Zealand*
[b] *Department of Physics and Astronomy, University of Canterbury, PB4800, Christchurch 8140, New Zealand*
[c] *The MacDiarmid Institute for Advanced Materials and Nanotechnology and Department of Physics and Astronomy, University of Canterbury, PB4800, Christchurch 8140, New Zealand*

Abstract

Infrared absorption has been used to determine the crystal-field levels of the $^2F_{7/2}$ excited multiplet of trivalent cerium doped into scheelite structure $LiYF_4$ single crystals. A crystal-field analysis well accounts for a total of six experimentally observed energy levels and the ground state g-values as previously determined by electron paramagnetic resonance, whilst intensity simulations confirm the experimentally assigned level symmetries. Temperature dependent spectral line broadening measurements highlight the importance of coupling to low frequency phonon modes of the YF_8 tetrahedron.

Keywords: $LiYF_4$, spectroscopy, crystal-field analyses, phonon scattering processes

1. Introduction

There has been much interest in trivalent cerium doped fluoride crystals, both fundamental spectroscopy (see for example, [1, 2, 3]) and with a view to applications such as the development of UV tunable lasers [4] or fast scintillators [5]. As a consequence, $LiYF_4$:Ce^{3+} has been the focus of many investigations, albeit

*Corresponding author
Email address: jon-paul.wells@canterbury.ac.nz (Jon-Paul R. Wells)

nearly exclusively optical measurements of interconfigurational transitions [6] or ground state electron paramagnetic resonance (EPR) studies [7]. However a large number of Ce^{3+} doped solid state gain media suffer from either strong excited state absorption (ESA) or ESA followed by the formation of pump induced photochromic centres [8] leading to poor laser performance in some cases.

$LiYF_4$ is a tetragonal crystal of the Scheelite structure ($CaWO_4$) having the C_{4h}^6 space group. In this material, each Li^+ ion is positioned at the centre of a tetrahedron of F^- ions and the Y^{3+} ions are each surrounded by eight F^- ions forming a tetragonal dodecaheron yielding D_{2d} point group symmetry. However, owing to a modest 2.3° distortion of the F^- cage the local Y^{3+} symmetry is in fact reduced to S_4.

In this work, we focus on the much less studied intra-$4f$ transitions occurring between the spin-orbit split $^2F_{5/2}$ and $^2F_{7/2}$ multiplets in the infrared region of the spectrum.

2. Experimental Details

Large single crystals of $LiYF_4$ doped with trivalent cerium were grown using the vertical Bridgman-Stockbarger technique [9, 10]. The furnace growth chamber was filled with greater than 1 atm pressure of highly purified argon gas to minimise evaporative losses. $LiYF_4$ incongruently melts at a temperature of 819 °C with a composition of 49 mol % YF_3 and 51 mol % LiF. The crystal growth was unseeded in graphite crucibles and the as grown boules were unoriented.

Infrared absorption spectra were recorded at 0.25 cm^{-1} resolution using a Bio-Rad FTS 40 Fourier transform infrared spectrometer. The crystal samples were cooled by thermal conduction with the 10 K stage of a CTS LTS 0.1 closed cycle helium cryostat with a temperature control unit regulating the current through a resistive heater placed at the back of the cold stage head.

3. Results and Discussion

3.1. Infrared Absorption Spectra

Figure 1 shows the 10 K infrared absorption spectrum of a 4.3 mm thick sample of $LiYF_4$ doped with 0.5% Ce^{3+}. Transitions to the $^2F_{7/2}$ multiplet are observable in the 2000-3000 cm^{-1} region due to the spin-orbit splitting of the degenerate $4f^1$ configuration superimposed upon the crystal-field splitting of the excited multiplet. Under S_4 point group symmetry the $J = 7/2$ multiplet is expected to break up into two states of $\gamma_{5,6}$ symmetry and another two states of $\gamma_{7,8}$ symmetry. As such, we label the crystal-field levels with the usual notation of a letter with a numerical subscript (Z for the ground multiplet and Y for the excited multiplet; Z_1 denoting the ground state, Z_2 the first excited state and so on) and the appropriate irreducible representation.

All of the four expected transitions are clearly observed in figure 1(a). Additional structure observable in the spectrum is assigned to $LiYF_4$ host lattice phonon sidebands displaced from the 2216.1 cm^{-1}, $Z_1\gamma_{7,8} \rightarrow Y_1\gamma_{5,6}$ zero phonon, electronic transition consistent with those observed in previous optical studies of lanthanide doped $LiYF_4$ (see for example [11]). The most prominent of these corresponds to the 248 cm^{-1} $LiYF_4$ TO mode [12, 13]. Additional sharp peaks centred around 2350 cm^{-1} are residual atmospheric contamination observed as the CO_2 rotation-vibrational bands. These appear as a decrease in absorption due to imperfect ratio of the background and single beam absorption spectra by the FTIR spectrometer. Our infrared absorption results for $LiYF_4$:Ce^{3+} are essentially in agreement with those reported in an earlier study [14], albeit that our data is obtained at 10 K whilst that in [14] was limited to 100 K. We note that the 'extra lines in the 2800-2900 cm^{-1} region' commented on in [14] are simply grease on the surfaces of the sample.

3.2. Crystal-Field Analysis and Simulated Spectra

In order to unambiguously assign irreps to the Ce^{3+} energy levels from the transitions observed in the infrared spectrum, a crystal-field analysis was performed,

followed by a calculation of the expected transition intensities. To achieve this, we note that the energy of the $Z_2\gamma_{5,6}$ state has been determined to be 216 cm^{-1} from high resolution $4f^{n-1}5d \rightarrow 4f^n$ emission spectra [15] and the ground state g-values (magnetic splitting factors) are known from EPR [7]. As such our analysis is based upon fits to both the experimental energy level data and the g-values.

The effective Hamiltonian describing the energy levels of the Ce^{3+} ions has the form

$$H = H_{\mathrm{FI}} + H_{\mathrm{CF}} + H_{\mathrm{Z}}, \tag{1}$$

where H_{FI} corresponds to the free-ion term (and contains only the spin-orbit interaction), H_{CF} is the crystal-field Hamiltonian and H_{Z} represents the Zeeman interaction. The parametric Hamiltonian appropriate for S_4 symmetry is given by:

$$\begin{aligned} H_{\mathrm{CF}} =& B_0^2 C_0^2 + B_0^4 C_0^{(4)} + B_0^6 C_0^{(6)} + B_4^4 (C_4^{(4)} + C_{-4}^{(4)}) \\ &+ B_4^6 (C_4^{(6)} + C_{-4}^{(6)}) - i B_4^{6'} (C_4^{(6)} - C_{-4}^{(6)}) \end{aligned} \tag{2}$$

where B_q^k are the usual one electron crystal-field parameters and $C_q^{(k)}$ are the Racah spherical tensors expressed in the Wybourne normalisation [16]. The results are shown in tables 1 and 2. Our calculation used the $LiYF_4$:Pr^{3+} crystal-field parameters [17] as initial values in the calculation and fitting process.

Good approximation to the experimental energy levels and g-values is obtained with crystal-field parameters consistent with that of other rare-earth ions in $LiYF_4$ as well as the parameter restricted fit for Ce^{3+} performed by Peijzel et al. [15]. Additionally, by weighting the contributions to the least squares χ^2, it was possible to establish that an accurate fit to the g-values is essential in order to obtain crystal-field parameters that are consistent with the parameter trend established in reference [19]. A recent study [20] points out the contribution of $^2F_{7/2}$ Kramers doublets to the ground state wavefunction and therefore to calculation of the g-values. For trivalent cerium, this can only occur

Table 1: Experimental, fitted, and ab-initio [18] energy levels ($cm^{-1}\pm0.1$), ground state g-values for Ce^{3+} in $LiYF_4$.

State	Experiment	Fitted	Ab-initio
$Z_1\gamma_{7,8}$	0.0	1.5	0
$Z_2\gamma_{5,6}$	216	213.8	247
$Z_3\gamma_{7,8}$	-	414.4	481
$Y_1\gamma_{5,6}$	2216.1	2215.5	2214
$Y_2\gamma_{7,8}$	2312.8	2312.1	2255
$Y_3\gamma_{5,6}$	2428.8	2430.1	2409
$Y_4\gamma_{7,8}$	3157.8	3158.6	3016
$g_\parallel$	2.765	2.751	
$g_\perp$	1.473	1.514	

through crystal-field J_z-mixing and therefore its significance varies in different host crystals. For example, our analyses show that in $LiYF_4$ a 1% wavefunction admixture occurs in this fashion, however for the $C_{4v}(F^-)$ centres in CaF_2 and SrF_2 the ground state is a 100% pure $J = 5/2$ Kramers doublet.

Our parameters are consistent with those obtained for other lanthanide ions [17, 21], being similar to those for $LiYF_4$:Pr^{3+}, though those fits restricted the parameters to be real. Recent ab-initio calculations [18] use the correct site symmetry, with structure optimised via DFT calculations and energy levels and crystal-field parameters obtained from a sophisticated embedded-cluster calculation. The results given in Tables 1 and 2 show good agreement between the experimental and ab-initio energy levels and the fitted and ab-initio parameters. Figure 1(b) shows the simulated infrared absorption spectrum. The theoretical transition intensities were obtained by evaluating the matrix elements of the magnetic dipole operator using the wavefunctions calculated above. This allowed for the computation of the dipole strengths, and, by convolving the resulting individual Gaussian lineshapes of each transition, yielded the shown simulated spectrum. The full width at half maximum (FWHM) of individual

Table 2: Fitted and ab-initio [18] spin-orbit and S_4 symmetry crystal-field parameters (cm^{-1}) for Ce^{3+} in $LiYF_4$.

Parameter	Fitted	Ab-initio
ζ	626	-
B_0^2	298	310
B_0^4	-1328	-1104
B_4^4	-1282	-1418
B_0^6	-192	-70
B_4^6	-1743	-1140
$B_4^{6'}$	693	237

Gaussians were estimated from the experimental spectrum.

3.3. Spectral Line Broadening

The effect of electron-phonon coupling on the spectral lines of optically active ions in solids is to increase the spectral linewidths and to induce a temperature dependence in the spectral line position [22]. The temperature dependent spectral linewidth has contributions from inhomogeneous broadening $\Delta\nu_{\rm inh}$ (which is temperature independent, arising from strains and defects in the host lattice) as well as all processes contributing to the homogeneous (or dynamic) linewidth, $\Delta\nu_{\rm hom}$. The homogeneous linewidth is determined by population relaxation (such as radiative or non-radiative decay) as well as dephasing processes such as elastic phonon scattering (often termed the 'Raman process' in the literature [14]). Detailed models of the electron-phonon interaction for lanthanide ions have been developed [23] and applied to interconfigurational $4f^n \rightarrow 4f^{n-1}5d$ transitions observed for several ions in $LiYF_4$ [24]. Here we employ a simple and commonly used model which highlights the essential physics. For the infrared transitions of Ce^{3+}, we model the temperature dependent contribution from population relaxation as direct multiphonon emission and phonon absorption between the levels of the $^2F_{7/2}$ multiplet. This gives rise to an expression

of the form:

$$\Delta\nu = \Delta\nu_{\rm inh} + \alpha\left(\frac{T}{T_D}\right)^7 \int_0^{T_D/T} \frac{x^6 e^x}{(e^x-1)^2} dx + \sum_{j<i} \beta_{ij}\left[\prod_p (n_p+1)\right] + \sum_{j>i} \beta_{ij} n_k \tag{3}$$

where $x = \hbar\omega/kT$. n_p and n_k are the Bose-Einstein occupation numbers of the p- and k- th phonon modes, respectively, which are equal to $[\, e^{\hbar\omega/kT} - 1]^{-1}$. Furthermore, T_D is the Debye temperature defined by $kT_D = \hbar\omega_{\rm cutoff}$ with $\omega_{\rm cutoff}$ being the $LiYF_4$ phonon cutoff frequency of around 570 cm^{-1} [12]. Here we will adopt a value, inferred from the elastic constants of the crystal, of 403 K [25]. The lower value of the Debye temperature reflects the deviation of real crystals from the Debye model, in particular, the significance of low energy phonons. The electron-phonon coupling constants α and β_{ij} were determined by fitting to the linewidths as a function of temperature; the linewidths themselves were obtained by using the Win-IR curve-fitting routine built into the Digilab FTIR spectrometer's control software.

Figure 2(a) shows the temperature dependence of the FWHM of the 2216.1 cm^{-1} $Z_1\gamma_{7,8} \rightarrow Y_1\gamma_{5,6}$ transition. The measured 10 K linewidth of this lowest frequency transition is 0.48 cm^{-1}, a value which we adopt as the inhomogeneous width. Attempts to account for the data including only the Raman dephasing process do not give a good agreement and it might be expected that inclusion of $\hbar\omega$=96.7 cm^{-1} phonon absorption between the $Y_1\gamma_{5,6}$ and $Y_2\gamma_{7,8}$ levels improves the fit. The appropriate electron-phonon coupling constant $\beta_{1,2}$ is in fact set by the 10 K linewidth of the 2312.8 cm^{-1} $Z_1\gamma_{7,8} \rightarrow Y_2\gamma_{7,8}$ transition since the phonon emission and absorption processes have analytical forms which differ only in their temperature dependencies (i.e. $\beta_{1,2}$=$\beta_{2,1}$). Therefore, if the inhomogeneous width is assumed to be comparable to the $Z_1\gamma_{7,8} \rightarrow Y_1\gamma_{5,6}$ transition, the upper limit of $\beta_{1,2}$=1.8 cm^{-1}. This is plotted as a long-dashed line in figure 2(a) for α=1000 cm^{-1}, T_D=403 K and $\beta_{1,2}$=1.8 cm^{-1}. It can be seen on the semi-log scale of figure 2 that this is not a good approximation to the data.

If $\beta_{1,2}$ is allowed to vary freely, the data can be accounted for. However the fit results yield α=550 cm^{-1} and $\beta_{1,2}$=17 cm^{-1} which would suggest the sample is not in thermal equilibrium; this is unphysical. The addition of absorption to the higher lying $Y_3\gamma_{5,6}$ state will not improve the fit owing to the energy gap of $\Delta E_{1,3}$=212.7 cm^{-1}, which requires a phonon population at energies that is not active at sufficiently low temperatures.

Ellens et al. [14] adopt a Debye temperature of T_D=250 K for $LiYF_4$ in their comparative study of electron-phonon coupling for lanthanide ions. Using this very low Debye temperature we obtain the short-dashed line in figure 2(a) for α=280 cm^{-1} and a direct 96.7 cm^{-1} phonon absorption with $\beta_{1,2}$=1.8 cm^{-1}. As can be seen this yields an improvement; however, the low temperature data is poorly approximated. Given the apparent significance of low energy phonons, and in order to account for the data, we abandon the Debye model and consider Raman dephasing processes involving a single phonon mode. In this case we may write for the second term in equation (3):

$$\alpha\left(\frac{T}{T_D}\right)^7 \int_0^{T_D/T} \frac{x^6 e^x}{(e^x-1)^2} dx = \alpha n_\omega (n_\omega + 1) \tag{4}$$

with n_ω the appropriate Bose-Einstein factor. Following [13], we note that for $LiYF_4$ vibrations in the 0-200 cm^{-1} frequency range involve ions of the YF_8 tetrahedron and, significantly, are affected by substitution of Y^{3+} by trivalent lanthanides. By contrast, the highest frequency modes essentially involve motion of the Li^+ ions alone. We here adopt a phonon energy of $\hbar\omega$=105 cm^{-1}, inferred from optical spectroscopy [11] and the weak phonon sidebands observed here in absorption for Ce^{3+}. The solid line in figure 2(a) corresponds to a fit assuming the Raman dephasing process occurs via a single phonon of frequency 105 cm^{-1} with α=21 cm^{-1} and including phonon absorption between the Y_1 and Y_2 states as previously. As can be seen a good agreement is obtained, which suggests this transition is strongly coupled to low frequency phonons associated with the motion of the yttrium ion itself.

The two remaining strong transitions at 2313.8 and 3158.6 cm^{-1} have successively greater widths of 2.25 cm^{-1} and 12.2 cm^{-1}, respectively, due to fast,

intra-multiplet non-radiative relaxation. Figure 2(b) shows the temperature dependence of the linewidth of the 2312.8 cm^{-1} $Z_1\gamma_{7,8}$ $\rightarrow Y_2\gamma_{7,8}$ transition. Unfortunately data could only be reliably obtained to 150 K due to the close proximity to the atmospheric CO_2 absorption bands. This limits the usefulness of the data. Adopting 0.48 cm^{-1} as the inhomogeneous linewidth, the remaining $\sim$1.8 cm^{-1} is set by phonon emission between $Y_2\gamma_{7,8}$ and $Y_1\gamma_{5,6}$ and (as discussed above) determines the coupling constant, $\beta_{2,1}$. Two different fit curves are shown in figure 2(b). The dashed line corresponds to elastic scattering at a single phonon frequency at 105 cm^{-1} with α=15 cm^{-1} as well as phonon emission to the $Y_1\gamma_{5,6}$ state and $\hbar\omega$=116 cm^{-1} phonon absorption to $Y_3\gamma_{5,6}$ with $\beta_{2,3}$=12 cm^{-1}. The solid line is again the Raman scattering process but assuming a Debye distribution with T_D=403 K as previously, and with phonon absorption having $\beta_{2,3}$=15 cm^{-1} and emission having $\beta_{2,1}$=1.8 cm^{-1}. With such limited data it is hard to draw any meaningful conclusions.

The $Z_1\gamma_{7,8}$ $\rightarrow Y_4\gamma_{7,8}$ transition at 3158.8 cm^{-1} has a low temperature linewidth determined by multiphonon emission. Assuming an inhomogeneous linewidth of 0.48 cm^{-1}, and making the approximation that the primary non-radiative decay pathway is a two phonon decay to the $Y_3\gamma_{5,6}$ level 729 cm^{-1} lower in energy, we set $\beta_{4,3}$=11.7 cm^{-1}. The dashed line in figure 2(c) is a fit including decay into two equal energy phonons at 364.5 cm^{-1} with the inclusion of the Raman process assuming a Debye distribution having T_D=403 K as previously and with α=550 cm^{-1}. Again this underestimates the activation temperature. By contrast, the solid line (which differs only in that the Raman dephasing process is set to occur through a single phonon mode at 105 cm^{-1}) fits the data reasonably well for α=11.5 cm^{-1}.

4. Conclusions

Combining infrared absorption as well as previously measured high resolution inter-configurational emission and EPR data, we have performed a crystal-field analysis for the $4f$ levels of Ce^{3+} in $LiYF_4$. Excellent agreement is obtained for

fits to the six experimentally determined energy levels as well as the ground state g-values, with the resultant crystal-field parameters in line with those for other lanthanide ions in this host crystal. An intensity analysis has been employed to confirm the irrep assignments used in the fits, and has been found to yield a good agreement with the infrared absorption data to the $^2F_{7/2}$ multiplet.

Temperature dependent infrared absorption has been used to investigate the dynamic linewidth via thermally induced spectral line-broadening. The data indicates the importance of low frequency motion involving ions of the YF_8 tetrahedron. An alternative interpretation assuming a Debye model for the phonon density of states, and utilising a Debye temperature inferred from elastic constants, yields values for the electron-phonon coupling constants which are unrealistically large (in fact comparable to or larger than those obtained for transition metal ions such as Co^{2+} [26]).

Acknowledgements

This work was supported by the Marsden Fund of the Royal Society of New Zealand under research contract 09-UOC-080. S.P.H. acknowledges the support of the University of Canterbury through the award of a postgraduate scholarship.

References

[1] J. M. W. Verwaij, C. Pedrini, D. Bouttet, C. Dujardin, H. Lautesse, B. Moine, Fluorescence of Ce^{3+} in $LiREF_4$ (RE=Gd, Yb), Optical Materials 4 (1997) 575–582.

[2] M. Yamaga, T. Inoue, S. Yabashi, M. Honda, J. P. R. Wells, K. Shimamura, T. Fukuda, Site symmetry and crystal-field splittings of Ce^{3+} in $LiLuF_4$ and $LiSr_{0.8}Ca_{0.2}AlF_6$, Radiation Effects and Defects in Solids 157 (2002) 977–982.

[3] V. V. Pavlov, M. A. Marisov, V. V. Semashko, A. S. Nizamutdinov, L. A. Nurtinova, S. L. Korableva, A new technique of the excited state photoin-

onization studies in Ce:$LiYF_4$ and Ce:$LiLuF_4$ crystals, J. Lumin. 133 (2013) 73–76.

[4] F. Okada, S. Togawa, K. Ohta, S. Koda, Solid state ultraviolet tunable laser: A Ce^{3+} doped $LiYF_4$ crystal, J. App. Phys. 75 (1994) 49–53.

[5] C. M. Combes, P. Dorenbos, C. W. E. van Eijk, C. Pedrini, H. W. Den Hartog, J. Y. Gesland, P. A. Rodnyi, Optical and scintillation properties of Ce^{3+} doped $LiYF_4$ and $LiLuF_4$, J. Lumin. 71 (1997) 65–70.

[6] N. Kodama, M. Yamaga, B. Henderson, Energy levels and symmetry of Ce^{3+} in fluoride and oxide crystals, J. App. Phys. 84 (1998) 5820–5822.

[7] T. Yosida, M. Yamaga, D. Lee, T. P. J. Han, H. G. Gallagher, B. Henderson, The electron spin resonance and optical spectra of Ce^{3+} in $LiYF_4$, J. Phys.: Condens. Matter 9 (1997) 3733–3739.

[8] K. S. Lim, D. S. Hamilton, Optical gain and loss studies in Ce^{3+}:$YLiF_4$, J. Opt. Soc. Am. B. 6 (1989) 1401.

[9] W. A. Shand, Growth of $LiYF_4$, J. Crys. Growth 5 (1969) 143.

[10] S. Duffy, J. P. R. Wells, H. G. Gallagher, T. P. J. Han, Bridgman growth and laser excitation of $LiYF_4$:Sm^{3+}, J. Crys. Growth 203 (1999) 405.

[11] J. P. R. Wells, M. Yamaga, T. P. J. Han, H. G. Gallagher, M. Honda, Polarized laser excitation, electron paramagnetic resonance and crystal-field analyses of Sm^{3+} -doped $LiYF_4$, Phys. Rev B. 60 (1999) 3849.

[12] S. A. Miller, H. E. Rast, H. H. Caspers, Lattice vibrations of $LiYF_4$, J, Chem. Phys. 52 (1970) 4172.

[13] S. Salaün, A. Bulou, M. Rousseau, B. Hennion, J. Y. Gesland, Lattice dynamics of fluoride scheelites: II. inelastic neutron scattering in $LiYF_4$ and modelization, J. Phys.: Condens. Matter 9 (1997) 6957.

[14] A. Ellens, H. Andres, M. L. H. ter Heerdt, R. T. Wegh, A. Meijerink, G. Blasse, Spectral-line-broadening study of the trivalent lanthanide ion series. II. the variation of the electron-phonon coupling strength through the series, Phys. Rev. B. 55 (1997) 180.

[15] P. S. Peijzel, P. Vergeer, A. Meijerink, M. F. Reid, L. A. Boatner, G. W. Burdick, $4f^{n-1}5d \rightarrow 4f^n$ emission of Ce^{3+}, Pr^{3+}, Nd^{3+}, Er^{3+} and Tm^{3+} in $LiYF_4$ and YPO_4, Phys. Rev. B. 71 (2005) 045116.

[16] B. G. Wybourne, Spectroscopic properties of rare earths, Wiley Interscience Publishers, 1965.

[17] L. Esterowitz, F. J. Bartoli, R. E. Allen, D. E. Wortman, C. A. Morrison, R. P. Leavitt, Energy levels and line intensities of Pr^{3+} in $LiYF_4$, Phys. Rev. B. 19 (1979) 6442.

[18] J. Wen, L. Ning, C. Duan, Y. Chen, Y. Zhang, M. Yin, A theoretical study of the structural and energy spectral properties of Ce^{3+} ions doped in various fluoride compounds, J. Phys. Chem. C 116 (2012) 20513.

[19] L. van Pieterson, M. F. Reid, R. T. Wegh, S. Soverna, A. Meijerink, $4f^n \rightarrow 4f^{n-1}5d$ transitions of the light lanthanides: Experiment and theory, Physical Review B 65 (4) (2002) 045113.

[20] Y. Mei, W. C. Zheng, Y. G. Yang, Studies of the crystal-field energy levels and g factors for Ce^{3+} in $LiYF_4$, Optik 124 (2013) 3949.

[21] C. Görller-Walrand, K. Binnemans, Rationalization of crystal–field parameterization, in: J. K. A. Gschneidner, L. Eyring (Eds.), Handbook on the Physics and Chemistry of Rare Earths, Vol. 23, North-Holland, Amsterdam, 1996, p. 121.

[22] R. C. Powell, Physics of Solid-State Laser Materials, Springer-Verlag, New York, 1998.

[23] B. Z. Malkin, K. K. Pukhov, S. K. Saikin, E. I. Baibekov, A. R. Zakirov, Theoretical studies of non-radiative 4f-4f multiphonon transitions in dielectric crystals containing rare-earth ions, J. Molec. Struct. 838 (2007) 170.

[24] B. Z. Malkin, O. Solovyev, A. Y. Malishev, S. K. Saikin, Theoretical studies of electron-vibrational $4f^N$-$4f^{N-1}5d$ spectra in $LiYF_4$:RE^{3+} crystals, J. Lumin. 125 (2007) 175.

[25] S. E. Sarkisov, K. K. Pukhov, A. A. Kaminskii, A. G. Petrosyan, T. I. Butaeva, Manifestation of electron phonon interaction in insulating crystals doped with Pr^{3+} ions, Phys. Status Solidi A. 113 (1989) 193.

[26] A. P. Vink, A. Meijerink, G. D. Jones, Temperature dependence of infrared absorption lines of Co^{2+} in cadmium halides, Phys. Rev. B. 66 (2002) 134303.

Figure Captions

Figure 1: (a) 10 K infrared absorption spectrum of nominally unoriented $LiYF_4$:Ce^{3+} showing the $^2F_{5/2} \rightarrow ^2F_{7/2}$ transitions and (b) the simulated spectrum.

Figure 2: Temperature dependent line broadening for (a) the $Z_1\gamma_{7,8} \rightarrow Y_1\gamma_{5,6}$ transition, (b) the $Z_1\gamma_{7,8} \rightarrow Y_2\gamma_{7,8}$ transition and (c) the $Z_1\gamma_{7,8} \rightarrow Y_4\gamma_{7,8}$ transition, with fits to equation (3) either assuming a phonon density of states following a Debye distribution with T_D=403 K or a single phonon mode at 105 cm^{-1} (see text for further details).

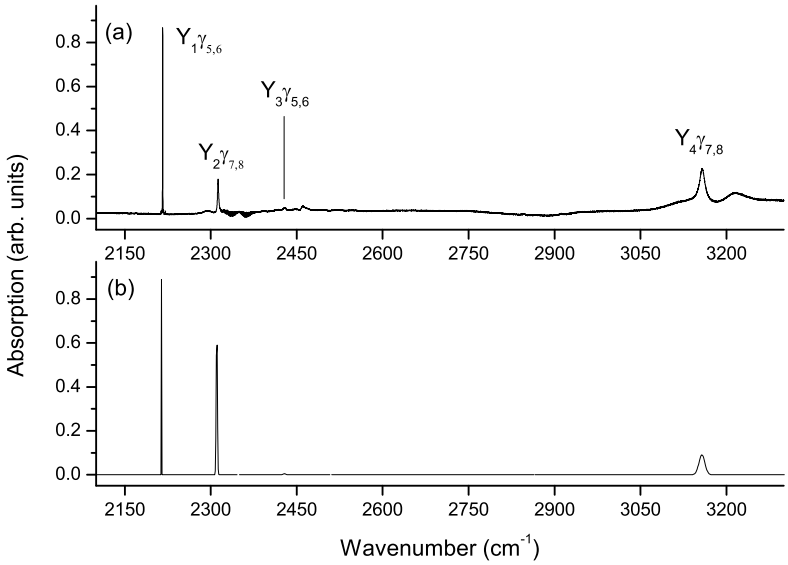
(a)
(b)
$Y_1\gamma_{5,6}$
$Y_3\gamma_{5,6}$
$Y_2\gamma_{7,8}$
$Y_4\gamma_{7,8}$
Absorption (arb. units)
Wavenumber (cm^{-1})
0.0
0.2
0.4
0.6
0.8
2150
2300
2450
2600
2750
2900
3050
3200

Figure 1:

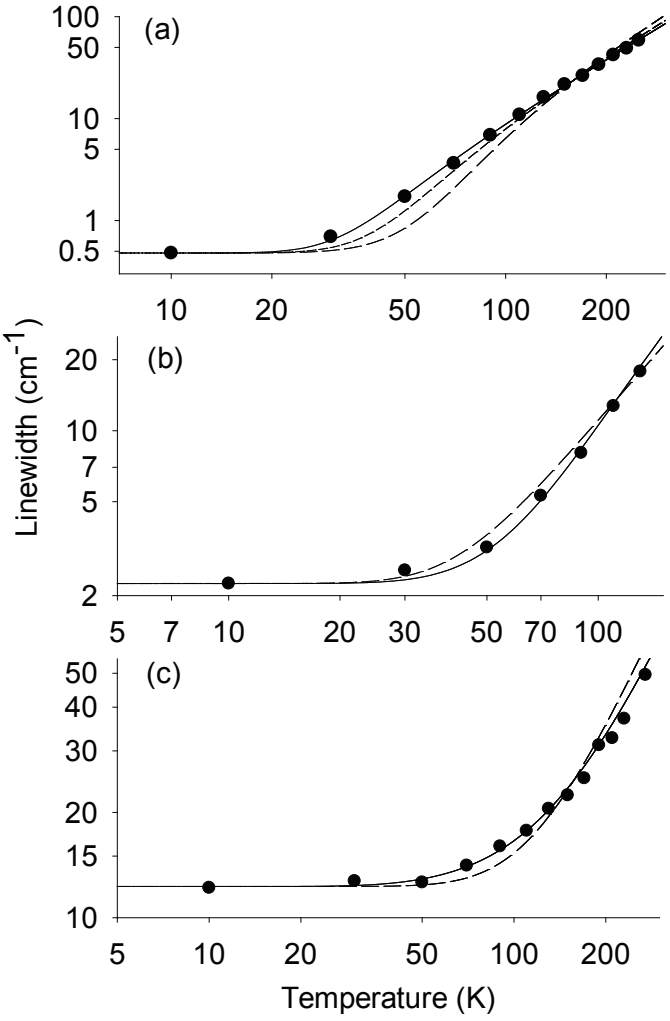
(a)
(b)
(c)
Linewidth (cm-1)
Temperature (K)
100
50
10
5
1
0.5
20
7
2
40
30
15
10
20
50
100
200
30
70

Figure 2: